Mechanics Research Communications 58 (2014) 124–132

Contents lists available at ScienceDirect

Mechanics Research Communications

journal homepage: www.elsevier.com/locate/mechrescom

Minimum mass design of tensegrity bridges with parametric architecture and multiscale complexity

R.E. Skelton [a], F. Fraternali [b,*], G. Carpentieri [b], A. Micheletti [c]

[a] UCSD, MAE/Aero, 9500 Gilman Dr., La Jolla, CA 92093, USA
[b] Department of Civil Engineering, University of Salerno, Fisciano (SA) 84084, Italy
[c] Dipartimento di Ingegneria Civile e Ingegneria Informatica, University of Rome "Tor Vergata", Rome (RM) 00133, Italy

ARTICLE INFO

Article history:
Received 19 June 2013
Received in revised form 19 October 2013
Accepted 22 October 2013
Available online 6 November 2013

Keywords:
Tensegrity structures
Form-finding
Minimum mass
Bridges
Parametric design
Multiscale complexity

ABSTRACT

We present a design methodology for tensegrity bridges, which is inspired by parametric design concepts, fractal geometry and mass minimization. This is a topology optimization problem using self-similar repetitions of minimal mass ideas from Michell (1904). The optimized topology is parametrized by two different complexity parameters, and two aspect angles. An iterative optimization procedure is employed to obtain minimum mass shapes under yielding and buckling constraints. Several numerical results are presented, allowing us to explore the potential applications. The given results show that the minimum mass complexity of the optimized bridge model has a multiscale character, being discrete with respect to the first complexity parameter, and markedly or infinitely large with respect to the second complexity.

1. Introduction

The subject of form-finding of tensegrity structures has attracted the attention of several researchers in recent years, due to the special ability of such structures to serve as controllable systems (geometry, size, topology and prestress control, cf, e.g., Tilbert and Pellegrino, 2011), and also because it has been recognized that the tensegrity architecture provides minimum mass structures for a variety of loading conditions, including structures subject to cantilevered bending load; compressive load; tensile load (under given stiffness constraints); torsion load; and simply supported boundary conditions (e.g. a bridge), without yielding and buckling (refer, e.g., to Skelton and de Oliveira, 2010a,b,c; Skelton and Nagase, 2012, and references therein). Other additional advantages of tensegrity structures over more conventional control systems are related to the possibility to integrate control functions within the design of the structure: in controlled tensegrity systems the mechanics of the controller and the structure can naturally cooperate, through the change of the configurational equilibrium of the structure, as opposed to traditional control systems, where often the control pushes against the equilibrium of the structure. It is also worth noting that it is possible to look at a tensegrity structure as a multiscale sensor/actuator, which features highly nonlinear dynamical behavior (geometrical and/or mechanical nonlinearities), and can be controlled in real time (Skelton and de Oliveira, 2010c; Fraternali et al., 2012).

Particularly interesting is the use of fractal geometry as a form-finding method for tensegrity structures, which is well described in Skelton and de Oliveira (2010a,b,c). Such an optimization strategy exploits the use of fractal geometry to design tensegrity structures, through a finite or infinite number of self-similar subdivisions of basic modules. It looks for the optimal values of suitable complexity parameters, according to given mechanical performance criteria, and generates admirable *tensegrity fractals*. The self-similar tensegrity design presented in Skelton and de Oliveira (2010a,b,c) is primarily focused on the generation of *minimum mass* structures, which are of great technical relevance when dealing, e.g., with tensegrity bridge structures (refer, e.g., to Bel Hadj Ali et al., 2010). The 'fractal' approach to tensegrity form-finding paves the way to an effective implementation of the tensegrity paradigm in *parametric architectural design* (Sakamoto et al., 2008; Rhode-Barbarigos et al., 2010; Phocas et al., 2012).

The present work deals with the parametric design of tensegrity bridges, through self-similar repetitions, at different scales of complexity. Michell (1904) derived the minimal mass topology when superstructures is only allowed above the roadbed. Deck design requires structure below the roadbed. Here we integrate the two to minimize mass of the total bridge. The design variables consist

* Corresponding author. Tel.: +39 089 964083; fax: +39 089 964045.
E-mail addresses: bobskelton@ucsd.edu (R.E. Skelton), f.fraternali@unisa.it (F. Fraternali), gcarpentieri@unisa.it (G. Carpentieri), micheletti@ing.uniroma2.it (A. Micheletti).

0093-6413/$ – see front matter © 2013 Elsevier Ltd. All rights reserved.
http://dx.doi.org/10.1016/j.mechrescom.2013.10.017

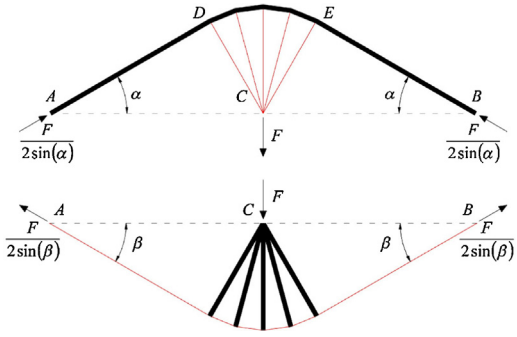

Fig. 1. Michell frames for a centrally loaded beam.

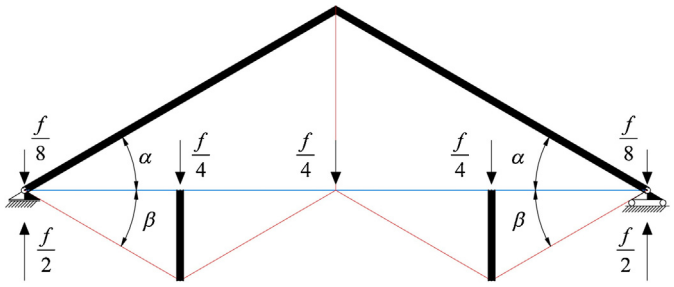

Fig. 2. Basic module of the tensegrity bridge ($n = 1$, $p = 1$). (For interpretation of the references to color in the text, the reader is referred to the web version of this article.)

of two complexity parameters and two aspect angles, which rule the geometry of the superstructure and the substructure. The iterative procedure proposed in Nagase and Skelton (2014) is employed to generate minimum mass shapes under yielding and buckling constraints, for varying values of the design variables. We begin by formulating the present bridge model in Section 2, and summarizing the employed minimization strategy in Section 3. Next, we present a variety of numerical results, which illustrate the potential of the proposed design strategy in generating minimum mass shapes of tensegrity bridges in association with different search landscapes (Section 4). A key result that we observe is that the minimum mass topology of the tensegrity bridge features two different (discrete–continuous) structural scales, which are related to the two employed complexity parameters. We end by presenting the main conclusions of the present study and future work in Section 5.

2. Tensegrity bridge model

In a famous work dated 1904, A.G.M. Michell examines the problem of finding the minimum volume network of fully stressed truss elements, which transmit a vertical force applied at the middle point C of a given segment AB to two fixed hinge supports applied at A and B (Michell, 1904). On pages 594–597 of this work, Michell deals with a truss network spanning a 2D continuous domain including the points A, B and C along its boundary (*centrally loaded beam*), and assumes that the material of such a domain is homogenous. Without entering the mathematical aspects of Michell's problem (refer, e.g., to Bouchittè et al., 2008), we notice that the Michell topology under consideration includes a portion DE of a circumference centered in C, the segments DA and EB lying on the tangents in D and F to the arch DE, and all the radii of the circular sector CDE (cf. Fig. 1, where the compressive elements (or *bars*) of the Michell frame are represented through thick black lines, while the tensile elements (or *strings*) are represented through thin red lines). Such a topology can be applied to both the regions placed above and below the applied force F, with the difference that the arch ADEB (hereafter also called Michell arch) works in compression and the radii pointing to C work in tension in the first case (Fig. 1, top), while, on the contrary, the arch ADEB works in tension and the radii pointing to C work in compression in the second case (Fig. 1, bottom). It is worth noting that the central angle of the circular sector CDE gets larger and larger, as the angle α (or β) gets closer and closer to 90° (Fig. 1).

We here introduce a parametric model of a tensegrity bridge obtained through n self-similar subdivisions of a basic module. This module is formed by a single Michell arch showing p radii, placed above the deck of the bridge, and two arches, each of them showing $q = p$ radii, placed below the deck. Such a bridge is constrained by a fixed hinge support at one end of the deck, and a rolling hinge support at the other end. We show the basic module corresponding to $n = p = 1$ in Fig. 2, while more complex shapes corresponding to higher values of n and p are shown in Fig. 3. Notice how each arch above the deck features p radii, and each arch below the deck features q radii, with $p = q$. The angles α and β can assume arbitrary values, and the horizontal elements at the level of the deck (represented through blue lines in Fig. 2) can work either in tension or in compression (*bidirectional elements*). Such elements provide the horizontal components of the lateral (supporting) forces of the Michell arch (Fig. 1). The basic module shown in Fig. 2 exhibits a single compressed arch above the deck, two tensile chords below the deck and a subdivision of the deck into four elements of equal length. Hereafter, we let f denote the total force transferred from the deck to the bridge structure. For $n > 1$, we assume that the elements of the nested arches placed above the deck can overlap each other. Moreover, to consider a common requirement for bridges over navigable water, we discard the outer arches placed below the deck (indicated by dotted lines in Fig. 3), in order to reduce the size of the substructure below the deck, for clearance above the water. In a real bridge structure, the elements placed above the deck would have a 3D geometry that prevents member overlapping. It is worth noting that the geometry corresponding to an arbitrary number n of self-similar subdivisions of the basic module features 2^{n+1} elements at the level of the deck, and show nodal forces equal to $f/(2^{n+1})$ in correspondence with the intermediate nodes placed at the level of the deck. The following variables completely define the geometry of the bridge structure: the total span L, the 'top aspect angle' α, the 'bottom aspect angle' β, and the complexity parameters n, p and q. The total numbers of top arches, n_{ta}, bottom arches, n_{ba}, strings, n_s, bars, n_b, and nodes, n_n, are given by:

$$n_{ta} = 2^n - 1, \quad n_{ba} = 2^n, \tag{1}$$

$$n_s = q n_{ta} + (p+1) n_{ba} + 2^{n+1}, \quad n_b = (q+1) n_{ta} + p n_{ba} + 2^{n+1}, \tag{2}$$

$$n_n = q n_{ta} + p n_{ba} + 2^{n+1} + 1. \tag{3}$$

As to the node coordinates, we observe that the nodes belonging to the 'superstructure' (i.e., the portion of the bridge placed above the deck) lie on n nested circumferences with radii R_{t_i} ($i = 1, \ldots, n$), while the nodes of the 'substructure' instead lie on sequential circumferences with radius R_b. Such radii are computed as follows

$$R_{t_i} = \frac{L}{2^i} \sin\alpha, \quad (i = 1, \ldots, n); \quad R_b = \frac{L}{2^n} \sin\beta. \tag{4}$$

We look for the optimal values of the complexity parameters n, p and q and the aspect angles α and β, which minimize the mass of the bridge under yielding and buckling constraints. As anticipated, we prescribe $q = p$ and we assume that all bars and strings are made up of the same material, for the sake of simplicity. The removal of such constraints is not a big issue from the theoretical point of view, but might lead to a significant increase in the number of optimization

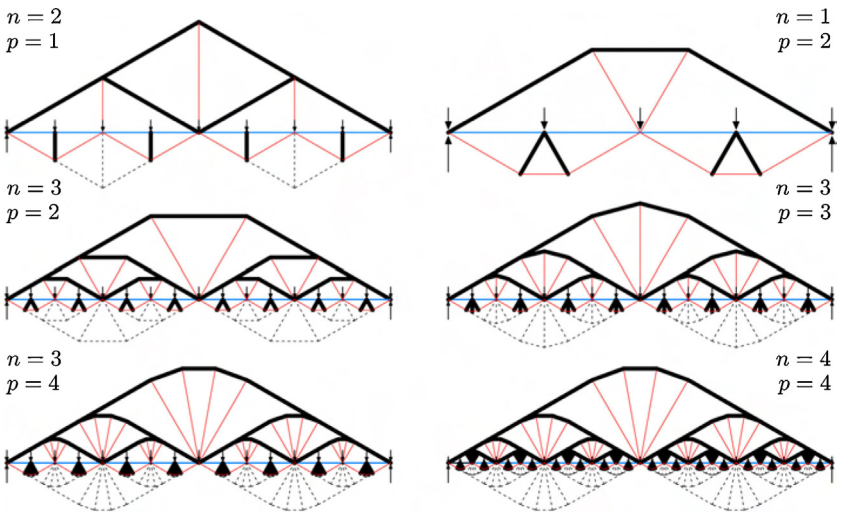

Fig. 3. Exemplary geometries of the tensegrity bridge for different values of the complexity parameters n and $p=q$.

variables. We close the present section with some remarks on prestress design, a typical feature of tensegrity systems. The procedure by Nagase and Skelton (2014) returns the minimal mass structure, for a given loading condition, together with a certain prestress state. By changing such a prestress, while increasing the mass, one can improve the ability of a structure to tolerate larger uncertainties in the external loading, and avoid slackening problems in cables. We leave the prestress calibration to a second step of the current design strategy, to be carried out after the minimal mass topology has been determined.

3. Mass minimization algorithm

We deal with the minimum mass design of the fractal bridge presented in Section 2 through the iterative linear programming procedure extensively presented in Nagase and Skelton (2014) that we briefly summarize hereafter. Let $\overline{\sigma}_Y$ denote the yield stress of the material. We enforce the following yield constraint in the generic string

$$\sigma_{s_i} = \overline{\sigma}_Y, \quad i = 1, \ldots, n_s, \tag{5}$$

where σ_{s_i} denotes the maximum admissible stress in such an element. Concerning the bars, we assume that the maximum admissible compressive stress σ_{b_i} in each of such elements, defined as a positive quantity, is given by

$$\sigma_{b_i} = \min(\overline{\sigma}_Y, \overline{\sigma}_{B_i}), \quad i = 1, \ldots, n_b, \tag{6}$$

where $\overline{\sigma}_{B_i}$ denotes the local buckling stress (Nagase and Skelton, 2014). Denoting the ith bar length by b_i, and assuming that such a bar has circular cross-section with radius r_{b_i}, we compute $\overline{\sigma}_{B_i}$ through Euler's formula

$$\overline{\sigma}_{B_i} = \frac{\pi^2 E}{4}\left(\frac{r_{b_i}}{b_i}\right)^2 = \frac{\pi E}{4}\frac{A_{b_i}}{b_i^2}, \quad i = 1, \ldots, n_b, \tag{7}$$

where E is the Young moduli of the material, and $A_{b_i} = \pi r_{b_i}^2$ is the area of the cross-section.

Now, let λ_{b_i} denote the compressive force per unit length in the ith bar, and let γ_{s_i} denote the tensile force per unit length in the ith string, both defined to be positive quantities. Assuming that all the bars and strings are *fully stressed* (i.e., the normal stress is equal to the maximum admissible stress in each of such elements), we compute the overall mass of the bridge structure through

$$m = \mathbf{c}^T\mathbf{x}, \tag{8}$$

with

$$\boldsymbol{x} = [\lambda_1 \cdots \lambda_{n_b} \mid \gamma_1 \cdots \gamma_{n_s}]^T, \tag{9}$$

$$\mathbf{c} = \begin{bmatrix} c_{b_1} & \ldots & c_{n_b} & | & c_{s_1} & \ldots & c_{n_s} \end{bmatrix}^T, \tag{10}$$

and we set

$$c_{b_i} = \frac{\rho b_i^2}{\sigma_{b_i}}, \quad c_{s_i} = \frac{\rho s_i^2}{\sigma_{s_i}}, \tag{11}$$

ρ being the mass density per unit volume of the material, and s_i being the length of the ith string. The force density vector $\mathbf{x}$ must satisfy the equilibrium equations of all the nodes of the bridge structure, which we write into the following matrix form

$$\boldsymbol{A}\boldsymbol{x} = \boldsymbol{w}. \tag{12}$$

Here, $\boldsymbol{A}$ is a *static matrix* depending on the geometry and the connectivity of bars and strings, and $\mathbf{w}$ is the *nodal force vector* obtained by stacking-up the single external force vectors of each node (Skelton and de Oliveira, 2010c). We neglect the contributions to $\mathbf{w}$ due to the self-weight of the bridge structure, assuming that the overall weight of the bridge structure is much less than the weight of the deck. If needed, the inclusion of gravity forces into Eq. (12) can be easily carried out following Nagase and Skelton (2014).

Given the bridge span, L, the total weight of the deck, f, and arbitrary values of the design variables, α, β, n and p, we determine the minimum bridge mass and the optimal values of the force densities by iteratively solving the linear programming problem

$$\begin{aligned} &\underset{\boldsymbol{x}}{\text{minimize}} \quad m = \boldsymbol{c}^T\boldsymbol{x}, \\ &\text{subject to} \quad \begin{cases} \boldsymbol{A}\boldsymbol{x} = \boldsymbol{w}, \\ \boldsymbol{x} \geq \mathbf{0}. \end{cases} \end{aligned} \tag{13}$$

Initally, we set $\sigma_{b_i} = \overline{\sigma}_Y$ in all the bars. Let us denote the current solution of problem (13) by $\boldsymbol{x}'$, and the corresponding minimum mass of the bridge by m' (step 1). The current values of the axial forces in all the bars and strings are given by

$$t'_{b_i} = \lambda'_{b_i} b_i, \quad t'_{s_i} = \gamma'_{s_i} s_i, \tag{14}$$

where λ'_{b_i} is the entry of $\boldsymbol{x}'$ corresponding to the ith bar, and γ'_{s_i} is the entry of the same vector corresponding to the ith string. By post-processing the current solution, and enforcing combined yielding

and buckling constraints in all the bars, we compute updated bar cross-section areas through

$$A''_{b_i} = \begin{cases} \sqrt{t'_{b_i}/(\pi E/4b_i^2)} & (t'_{b_i} \le t^*_{b_i}) \\ t'_{b_i}/\overline{\sigma}_Y & (t'_{b_i} > t^*_{b_i}) \end{cases}, \tag{15}$$

where $t^*_{b_i} = (\overline{\sigma}_Y)^2/(\pi E/4b_i^2)$ (Nagase and Skelton, 2014). Accordingly, we define an updated mass of the bridge structure, via the equation

$$m'' = \sum_{i=1}^{n_b} \rho A''_{b_i} b_i + \sum_{i=1}^{n_s} \frac{\rho s_i^2}{\sigma_{s_i}} x'_{s_i}. \tag{16}$$

If the ratio $|(m'' - m')/m'|$ is lower than a given tolerance we stop the optimization procedure at the current iteration, otherwise we set $\sigma_{b_i} = t'_{b_i}/A''_{b_i}$ and go back to step 1. The rest of the paper makes use of the following dimensionless mass factor,

$$\mu = \frac{m\overline{\sigma}_Y}{\rho L f}. \tag{17}$$

A pure yielding design of the bridge, which corresponds to the approach followed by Michell in his 1904 study of a centrally loaded beam, is obtained by arresting the above procedure at the first iteration ($\sigma_{b_i} = \overline{\sigma}_Y$ in all the bars). Hereafter, we use the index Y to denote the mass and the design variables corresponding to such a design strategy. It is worth noting that the solution of the optimization problem (13) leads us to resolve the indeterminacy associated with the bidirectional elements placed at the level of the deck (Nagase and Skelton, 2014).

4. Numerical results

In this section we present a collection of numerical results, which aim to illustrate the potential of the minimum mass design under consideration. We use the symbols μ^*, α^* and β^* to denote the minimum mass and the optimal aspect angles of the tensegrity bridge under combined yielding and buckling constraints, respectively, and the symbols μ^*_Y, α^*_Y and β^*_Y to denote the optimal values of the same quantities under simple yielding constraints. In all the examples, we search for a global minimum mass configuration of the bridge, by recursively running the optimization procedure presented in Section 3, so that the design variables n, p, α and β may range within prescribed search domains. We set the step increments of n and p to 1, the step increments of α and β to 0.01°. In addition, we set L, f and ρ to unity, in abstract units, and make use of the following assumptions: $\overline{\sigma}_Y = 6.9 \times 10^8 L^2/f$; $E = 2.1 \times 10^{11} L^2/f$. It is worth observing that the basic module shown in Fig. 2 can be in equilibrium either in presence of the elements placed at the level of the deck, or in absence of such elements (blue elements in Fig. 2), due to the double arch mechanism played by the two portions of the bridge placed above and below the deck. In order to highlight the relative 'weight' of the elements placed at the level of the deck, we introduce the following ratios,

$$\frac{\mu^*_{db}}{\mu^*_b}, \quad \frac{\mu^*_{ds}}{\mu^*_s}. \tag{18}$$

where μ^*_{db}, μ^*_{sb}, μ^*_b, μ^*_s denote the total mass of the bars placed at the level of the deck, the total mass of the strings placed at the level of the deck, the overall mass of the bars and the overall mass of the strings, respectively, in correspondence with any arbitrary minimum mass configuration under combined yielding and buckling constraints. We remind the reader that the elements placed at the level of the deck are bidirectional, in the sense that they can contemporarily serve as bars or strings (Nagase and Skelton, 2014).

Table 1
Selected results for the example in Section 4.1.

p	α^*_Y	β^*_Y	μ^*_Y	α^*	β^*	μ^*
1	41.83	24.11	1.1180	26.11	13.77	808.84
3	50.29	31.05	1.0235	42.78	24.83	446.26
5	53.42	33.97	0.9952	50.29	31.05	375.84
7	54.33	34.86	0.9896	51.97	32.59	349.79
9	54.42	34.95	0.9876	53.13	33.69	340.13
10	54.42	34.96	0.9871	53.42	33.97	338.30
11	54.44	34.97	0.9867	53.42	33.97	337.69
12	54.49	35.02	0.9864	53.42	33.97	337.92
13	54.53	35.06	0.9862	53.42	33.97	338.76
15	54.58	35.11	0.9859	53.13	33.69	341.67
20	54.65	35.18	0.9855	51.98	32.60	352.24
25	54.68	35.21	0.9854	74.39	22.29	375.03
30	54.70	35.23	0.9853	76.17	21.15	372.02
40	54.72	35.25	0.9852	78.37	19.60	369.85
50	54.72	35.25	0.9852	79.69	18.54	370.17
60	54.73	35.26	0.9851	80.57	17.75	371.58

4.1. Minimum mass design for n = 1, and variable p, α, and β

We begin by conducting a minimum mass design that keeps n constant and equal to 1, and lets α, β and p range in the following intervals,

$$p \in [1, 60], \quad \alpha \in (0, 90)^\circ, \quad \beta \in (0, 90)^\circ. \tag{19}$$

Fig. 4 and Table 1 show the optimization results obtained in the present case. Under simple yielding constraints, the results shown in Table 1 indicate that the mass of the bridge might converge to a global minimum when $p \to \infty$ ($\mu^*_Y \to 0.985$, cf. Table 1). Conversely, the aspect angles α and β converge to the following limiting values: $\alpha^*_Y \to 54.73^\circ$, and $\beta^*_Y \to 35.26^\circ$. The inclusion of self-weight (Nagase and Skelton, 2014) does not cause a significant change of the optimal topology: by adding gravity forces we indeed obtain $\mu^*_Y = 0.9853$, $\alpha^*_Y = 55.31^\circ$, $\beta^*_Y = 35.84$, when $p = 60$. Under *combined* buckling and yielding constraints, the mass of the bridge approaches a global minimum for a finite value of the complexity p ($\mu^* \to 337.69$ for $p = 11$, cf. Table 1). As p approaches such an optimal value, the aspect angles converge to the following limiting values: $\alpha^* \to 53.42^\circ$, and $\beta^* \to 33.97^\circ$. It is worth noting that the minimum mass configuration under combined buckling and yielding constraints shows similar aspect ratios and a much greater mass, as compared to that corresponding to simple yielding constraints. For $p < 25$, the mass ratio μ^*_{ds}/μ^*_s assumes values ranging in the interval $[1 \times 10^{-7}, 6 \times 10^{-5}]$, while the mass ratio μ^*_{db}/μ^*_b ranges in the interval $[2 \times 10^{-11}, 6 \times 10^{-7}]$. Such results show that the elements placed at the level of the deck can be ignored for $p < 25$. On the contrary, for $p \ge 25$ we again observe $\mu^*_{ds}/\mu^*_s \ll 1$, but this time the ratio μ^*_{db}/μ^*_b becomes relevant and progressively increasing with p, being equal to 0.56 for $p = 25$, and 0.68 for $p = 60$. The latter results highlight that the elements placed at the level of the deck act as compressed members (bars) of relevant structural importance for $p \ge 25$. Fig. 4 illustrates the geometries of the (relative) minimum mass configurations corresponding to several selected values of p, in presence of combined yielding and buckling constraints.

4.2. Minimum mass design for variable n, p, α, and β

The second minimum mass design that we examine assumes that all the design variables n, p, α, and β may simultaneously vary within the following bounds,

$$n \in [2, 5], \quad p \in [1, 7], \quad \alpha \in (0, 90)^\circ, \quad \beta \in (0, 90)^\circ. \tag{20}$$

The most relevant results corresponding to the present case are illustrated in Table 2 and Figs. 5 and 6. The results in Table 2 highlight that the global minimum mass configuration under

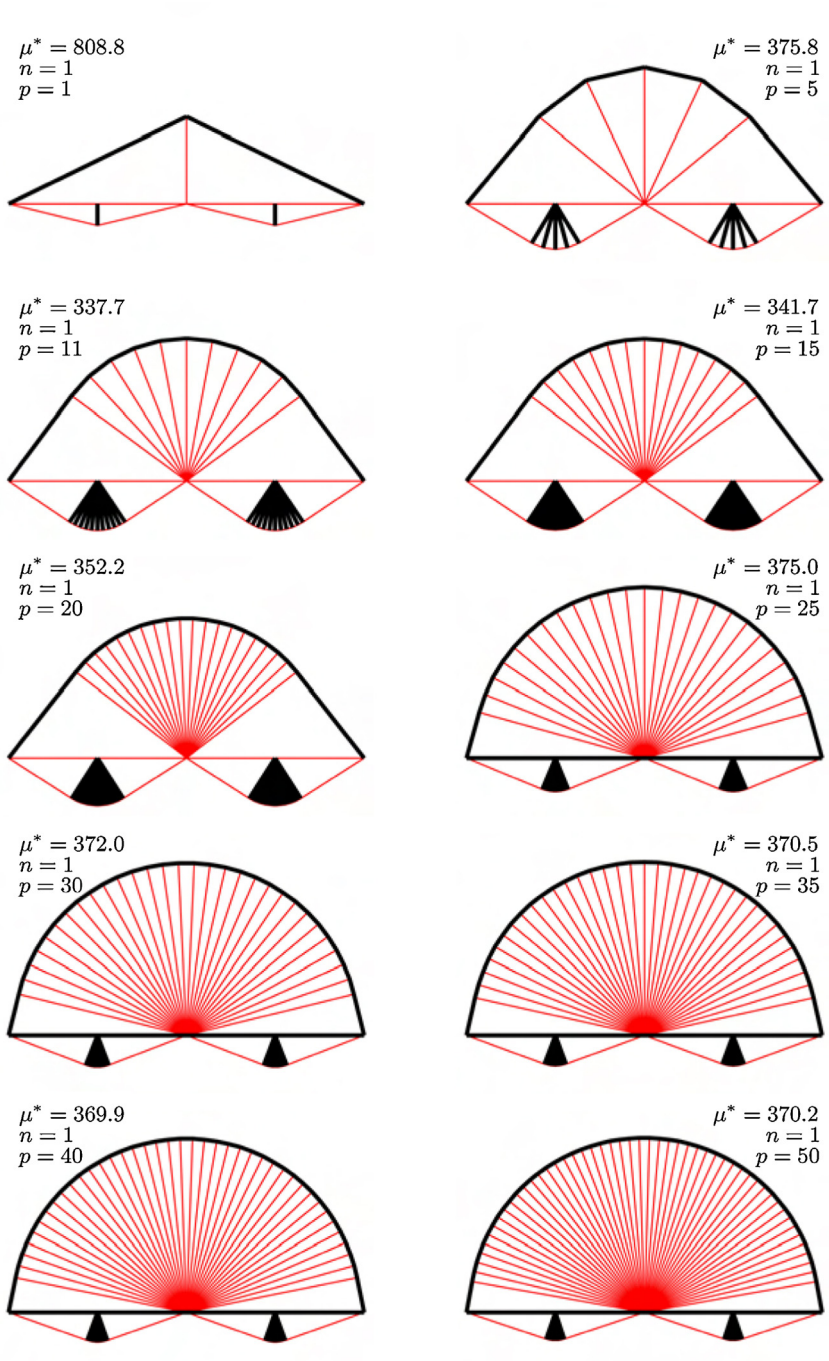

Fig. 4. Optimal bridge topologies under combined yielding and buckling constraints, for $n = 1$, $\alpha \in (0, 90)^\circ$, $\beta \in (0, 90)^\circ$, and $p \in [1, 50]$.

combined yielding and buckling constraints is reached for $n = 2$, $p = 7$ ($\mu^* = 333.17$, $\alpha^* = 62.52^\circ$, $\beta^* = 17.77^\circ$), within the search domain (20). In particular, the mass of such a configuration is slightly lower than the global minimum mass obtained for $n = 1$, $p = 11$ in Section 4.1 ($\mu^* = 333.17$ vs $\mu^* = 337.69$, respectively). Referring to the case with $n = 2$, in order to detect if the global minimum mass configuration is obtained for finite complexity p or not, we let this parameter grow up to $p = 13$, and determine the corresponding relative minimum mass configurations of the bridge. We find out that the mass of the bridge monotonically decreases when p grows from 1 to 13, and n remains equal to 2. In particular, the relative minimum mass configuration for $n = 2$ and $p = 13$ is the following: $\mu^* = 225.98$, $\alpha^* = 69.45^\circ$, $\beta^* = 23.97^\circ$. Such results, together with those presented in Table 2, indicate that the global minimum mass configuration of the bridge might be achieved either for rather large values of p, or in the limit $p \to \infty$, when $n \geq 2$. By adding gravity forces (Nagase and Skelton, 2014), and referring to the case with $n = 2$ and $p = 13$, we obtain $\mu^* = 227.49$, $\alpha^* = 69.48^\circ$, and $\beta^* = 23.52^\circ$. Such results show that the inclusion of self-weight does not cause a significant change of the minimum mass configuration at hand, as we already observed in presence of simple yielding constraints (cf. Section 4.1). As to the elements placed at the level of the deck, we observe the following results: $\mu^*_{db}/\mu^*_b \ll 1$, and $\mu^*_{ds}/\mu^*_s \ll 1$, for $n \leq 3$. The ratio μ^*_{ds}/μ^*_s becomes relevant for $n > 3$, being equal to 0.06 for $n = 4$ and $p = 1$, and 0.3 for $n = 5$ and $p = 1$. Nevertheless, the same ratio decreases with p for fixed n, being equal to $\approx 10^{-4}$

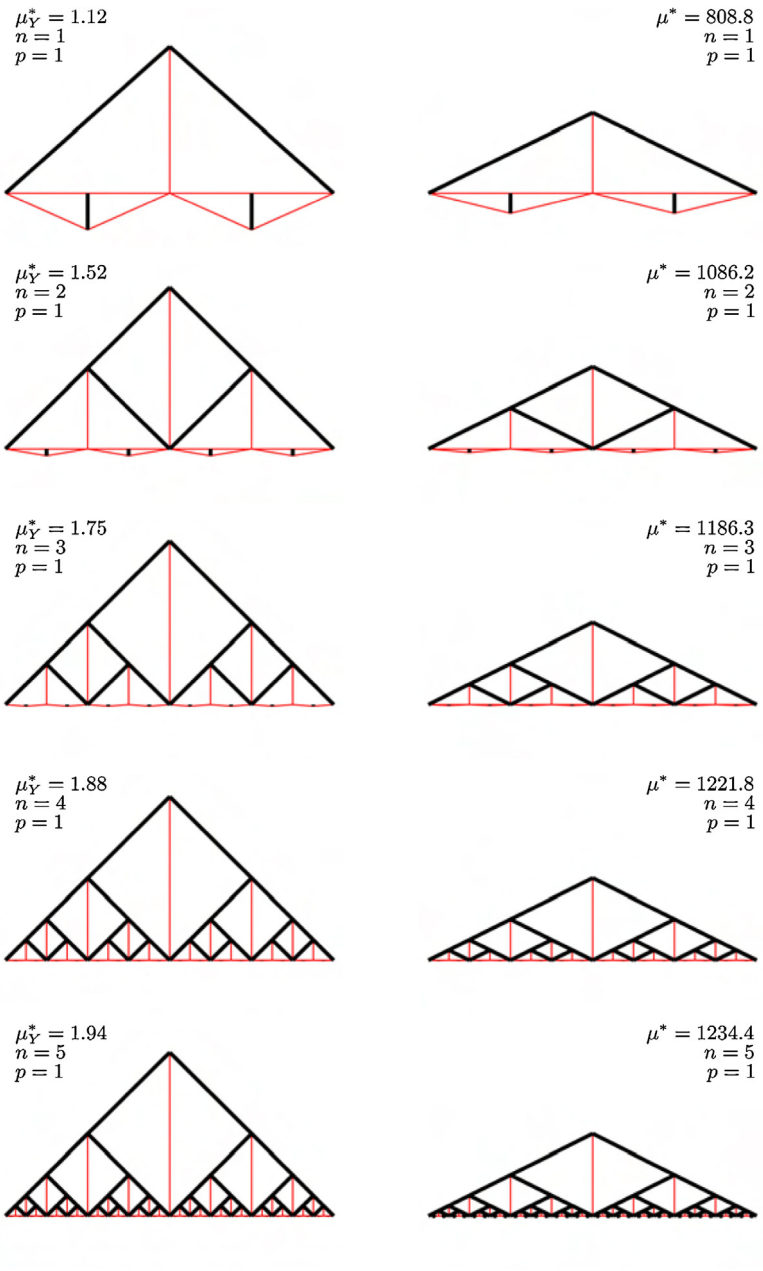

Fig. 5. Optimal topologies under yielding constraints (left) and combined yielding and buckling constraints (right) for different values of n and $p = 1$.

Table 2
Selected results for the example in Section 4.2.

n	p	α_Y^*	β_Y^*	μ_Y^*	α^*	β^*	μ^*
2	1	44.62	9.34	1.5207	26.58	4.77	1086.23
2	3	57.81	14.83	1.3329	45.20	9.53	558.02
2	5	63.73	18.66	1.2674	56.10	13.93	413.11
2	7	66.42	20.90	1.2534	62.52	17.77	333.17
3	1	44.96	4.08	1.7545	26.58	2.05	1186.33
3	3	59.52	6.92	1.5232	45.31	4.13	607.67
3	5	69.56	10.85	1.4341	56.63	6.19	446.20
3	7	72.52	12.78	1.4137	63.71	8.23	354.03
4	1	44.96	1.91	1.8761	26.58	1.03	1221.82
4	3	59.73	3.27	1.6256	45.31	1.93	625.75
4	5	71.41	5.66	1.5262	56.65	2.90	459.24
4	7	75.51	7.35	1.5021	63.82	3.88	363.95
5	1	45.01	0.93	1.9378	26.58	0.75	1234.39
5	3	59.92	1.60	1.6784	45.32	1.44	632.19
5	5	71.84	2.83	1.5747	56.65	1.71	463.95
5	7	76.80	3.96	1.5489	63.83	1.88	367.65

for $n = 4$ and $p = 7$, and $\approx 10^{-5}$ for $n = 5$ and $p = 7$. We can therefore conclude that such elements serve as tensile members (strings) for $n > 1$, and that their structural relevance increases with n and decreases with p. Regarding the global minimum mass configuration corresponding to the search domain (20) and simple yielding constraints, we observe that such a configuration is reached for $n = 2$ and $p = 7$ ($\mu_Y^* = 1.2534$, $\alpha_Y^* = 66.42^\circ$, $\beta_Y^* = 20.90^\circ$, cf. Table 2) and that the corresponding mass is greater than the global minimum obtained in Section 4.1 for $n = 1$ and $p \to \infty$ ($\mu_Y^* \to 0.9851$). It is also seen from Table 2 that, in each of the examined cases, the optimal values of α very slowly increase with n, and rather markedly increase with p. The optimal values of β instead markedly decrease with n, and significantly increase with p. It is worth noting that the two examined design strategies (simple yielding constraints and combined yielding and buckling constraints) lead to rather different aspect ratios of the bridge for $p = 1$ (cf. Fig. 5), and, on the contrary, to more similar geometries as p gets larger, for any given

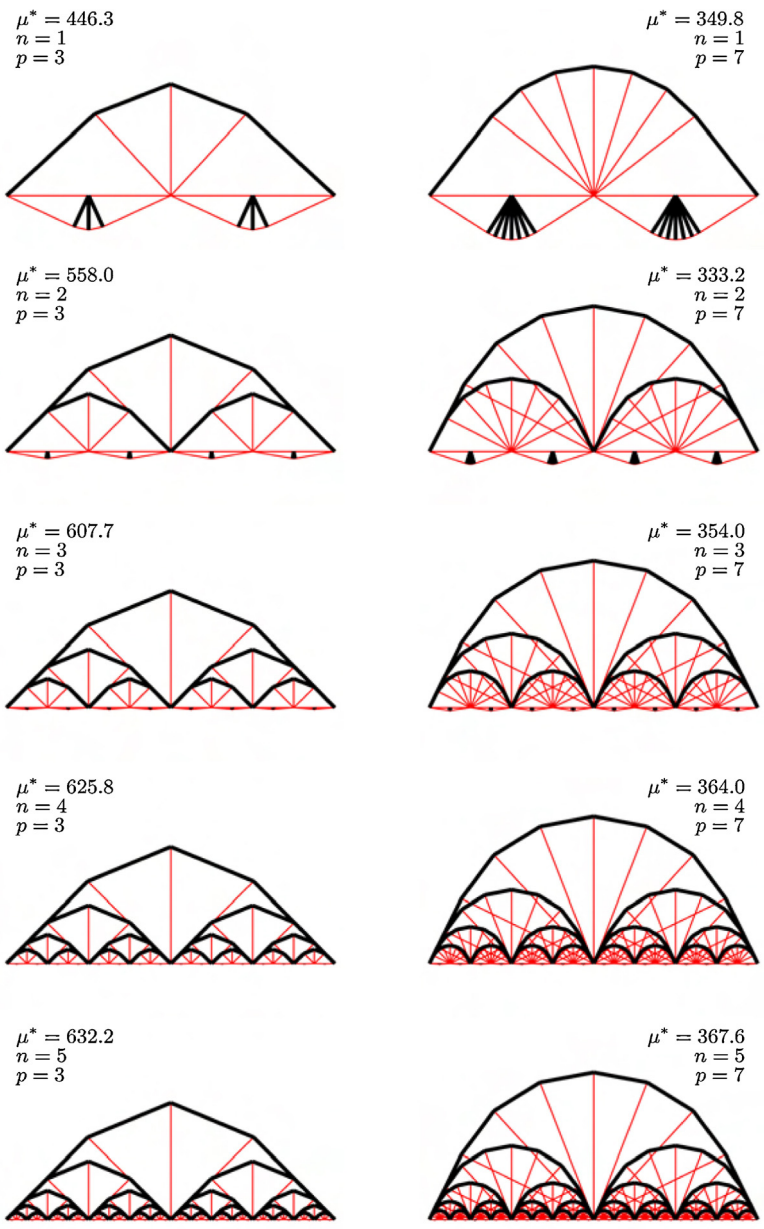

Fig. 6. Optimal topologies under combined yielding and buckling constraints for different values of n, $p = 3$ (left), and $p = 7$ (right).

n (cf. Table 2, and Section 4.1). The results shown in Fig. 6 emphasize that the current minimum mass design of the bridge leads to rather large values of α and considerably small values of β, as the complexity parameters n and p progressively increase. In particular, the bottom height of the bridge dramatical shrinks for $n \geq 3$ (Fig. 6). This is explained by observing that the lower chords of the bridge carry tensile forces $t_{ba} = f_n/2Sin(\beta)$ (cf. Fig. 1), with $f_n = f/(2^{n+1})$. As n goes to infinity and β goes to zero, it can be verified that t_{ba} approaches a finite limit. The solution with $\beta \to 0$ becomes convenient in terms of mass savings as $n \to \infty$, since it reduces the lengths of the tensile chords and compressed rays placed below the deck. We wish to remark, however, that the global minimum mass configuration is achieved for $n = 1$ under simple yielding constraints, and $n = 2$ under combined yielding and buckling constraints. Different results could be achieved by accounting for possible damage mechanisms of the deck, which are due, e.g., to material yielding or cracking (Schmidt et al., 2009), or excessive deflections.

4.3. *Minimum mass design for $n = 5$, $\alpha = 40^\circ$, $\beta = 60^\circ$, and variable p*

The results shown in Fig. 6 highlight that a rigorous minimum mass design of a tensegrity bridge might lead to rather disordered shapes and member overlapping. Moreover, bridge designers usually prefer to orient their conceptual designs, by requiring that the bridge features given aspect ratios, and/or given topologies or shapes. Therefore, it makes sense to consider a minimum mass design that keeps fixed most of the design variables, and lets just one of them to vary within prescribed bounds. Table 3 and Fig. 7 show the results of a minimum mass design that keeps $n = 5, \alpha = 40^\circ$, and $\beta = 60^\circ$ fixed, and lets the complexity p to range in the search interval $[1, 60]$. The results in Table 3 highlight that the mass of the bridge monotonically decrease with p within such a search domain, either under simple yielding constraints, and in presence of combined yielding and buckling constraints. The current results confirm

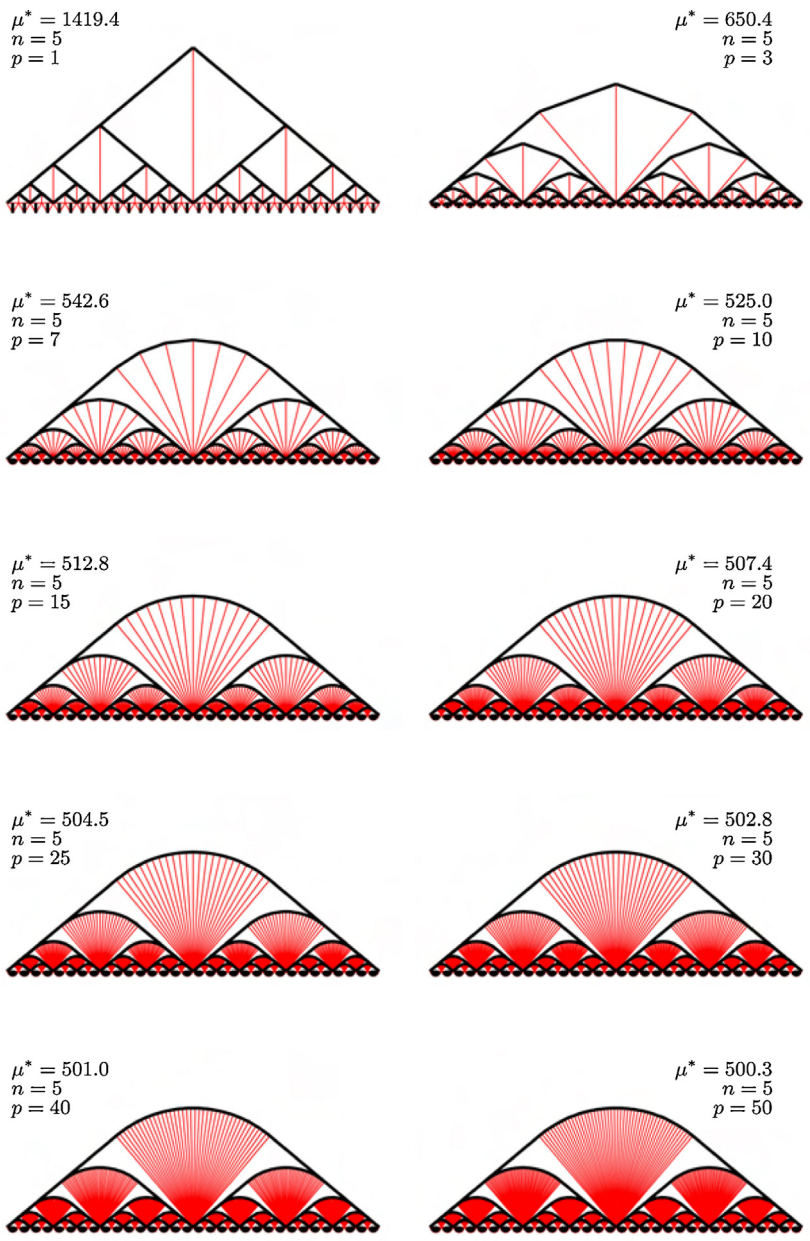

Fig. 7. Optimal topologies under buckling constraints for $n = 5$, fixed angles $\alpha = 40^\circ$ and $\beta = 60^\circ$, and different values of p.

Table 3
Selected results for the example in Section 4.3.

p	μ_Y^*	μ^*
1	2.0261	1419.43
5	1.8545	569.55
10	1.8486	524.96
15	1.8478	512.81
20	1.8475	507.41
30	1.8473	502.79
40	1.8473	501.03
50	1.8472	500.33
60	1.8472	500.12

those presented in the previous section, highlighting that the global minimum mass configuration is achieved either for very large values of p, or in the limit $p \to \infty$. Concerning the elements placed at the deck level, we now observe $\mu_{db}^*/\mu_b^* \ll 1$, and $\mu_{ds}^*/\mu_s^* \approx 0.6$, which implies that such elements serve as strings with relevant structural importance in the present case. Some of the relative minimum mass geometries corresponding to different choices of p are illustrated in Fig. 7.

5. Concluding remarks

We have presented a design methodology for tensegrity bridges, which is aimed to the generation of minimum mass shapes through parametric self-similar iterations. It makes use of basic units consisting of Michell trusses carrying a central point load (Michell, 1904; Baker et al., 2013; Sokóf and Rozvany, 2012); compressed arches above the deck level; and tensile cords below the deck. The proposed design procedure is ruled by two complexity parameters (n and p), two aspect angles (α and β), and admits either combined buckling and yielding constraints, or, as a special case, simple yielding constraints. The results presented in Section 4 point out that the global minimum mass configuration of the examined bridge model shows finite complexity n, and markedly large or infinite complexity p. We can therefore conclude that such a

bridge shows a multiscale, discrete–continuum complexity. In all the examined cases, we have observed that the minimum mass of the bridge under simple yielding constraints is about two orders of magnitude smaller than the minimum mass corresponding to combined buckling and yielding constraints. This implies that buckling failure cannot be ignored in practical applications of the present design methodology. Concerning the aspect ratios of the bridge, we have observed that, as the complexity n increases, the height of the portion of the bridge placed above the deck increases, while the height of the structure placed below the deck decreases dramatically. We wish to highlight that the present minimum mass designs cannot be understood as universal optima, under the given constraints. They indeed represent mass minimizers within the examined sets of bridge topologies, against which other bridge designs could be usefully compared to.

The present study opens the way for a variety of further applications of tensegrity structures in civil engineering and parametric architecture, where the tensegrity 'philosophy' has only been partially exploited at present (cf. also Bel Hadj Ali et al., 2010; Rhode-Barbarigos et al., 2010). Particularly challenging is the use of parametric tensegrity design for the next generation long span or pedestrian bridges, which might require smart structures based on lightweight materials, active or passive control strategies, and/or real-time structural health monitoring (Skelton, 2002). Tensegrity applications also calls for a robust design to take care of errors on members' manufactured lengths. These errors may lead to members' over-stressing and to a construction not replicating the exact theoretical structure, and could even produce instabilities. Developments in this direction constitute a ripe subject for future studies. We also address to future work the realization of real-scale or reduced-scale physical models of tensegrity bridges, as well as the 3D generalization of the proposed design approach. Further generalizations of the present study might regard the adoption of different objective functions (minimum compliance, fabrication and assembly cost, integrated mechanical, functional, and architectural performance criteria, etc.), the adoption of optimization strategies based on evolutionary form-finding methods (Fraternali et al., 2011; Yamamoto et al., 2011; Koohestani, 2012), or the lumped stress method (Fraternali et al., 2002; Fraternali, 2010), and an enlargement of the present numerical analysis to more complex search domains and real case studies. Regarding the adoption of a different objective function, we are currently refining computations by using a global cost function, where different contributions, such as the cost of material, fabrication, and assembly, are customarily weighted and summed together. An interesting challenge is the modeling of a trade-off between these different costs, since lightweight and easy-to-assemble components would also be more expensive to design and manufacture.

Acknowledgement

GC, FF, and RES acknowledge financial support from the Province of Avellino.

References

Baker, W.F., Beghini, L.L., Mazurek, A., Carrion, J., Beghini, A., 2013. Maxwell's reciprocal diagrams and discrete Michell frames. Struct. Multidisc Optim., http://dx.doi.org/10.1007/s00158-013-0910-0.

Bel Hadj Ali, N., Rhode-Barbarigos, L., Pascual Albi, A.A., Smith, I.F.C., 2010. Design optimization and dynamic analysis of a tensegrity-based footbridge. Eng. Struct. 32 (11), 3650–3659.

Bouchittè, G., Gangbo, W., Seppecher, P., 2008. Michell trusses and lines of principal action. Math. Mod. Methods Appl. Sci. 18, 1571–1603.

Fraternali, F., Angelillo, M., Fortunato, A., 2002. A lumped stress method for plane elastic problems and the discrete–continuum approximation. Int. J. Solids Struct. 39, 6211–6240.

Fraternali, F., 2010. A thrust network approach to the equilibrium problem of unreinforced masonry vaults via polyhedral stress functions. Mech. Res. Commun. 37, 198–204.

Fraternali, F., Marino, A., El Sayed, T., Della Cioppa, A., 2011. On the structural shape optimization through variational methods and evolutionary algorithms. Mech. Adv. Mater. Struc. 18, 224–243.

Fraternali, F., Senatore, L., Daraio, C., 2012. Solitary waves on tensegrity lattices. J. Mech. Phys. Solids 60, 1137–1144.

Koohestani, K., 2012. Form-finding of tensegrity structures via genetic algorithm. Int. J. Solids Struct. 49, 739–747.

Michell, A.G.M., 1904. The limits of economy of material in frame-structures. Philos. Mag. 8, 589–597.

Nagase, K., Skelton, R.E., 2014. Minimal mass design of tensegrity structures. In: Proceedings of "Sensors and Smart Structures Technologies for Civil, Mechanical, and Aerospace Systems" conference, a part of SPIE Smart Structures/NDE 2014, 9–13 March, 2014, Town & Country Resort and Convention Center, San Diego, California, United States, Paper No. 9061-75.

Phocas, M.C., Kontovourkis, O., Matheou, M., 2012. Kinetic hybrid structure development and simulation. Int. J. Archit. Comput. 10 (1), 67–86.

Rhode-Barbarigos, L., Jain, H., Kripakaran, P., Smith, I.F.C., 2010. Design of tensegrity structures using parametric analysis and stochastic search. Eng. Comput. 26 (2), 193–203.

Sakamoto, T., Ferrè, A., Kubo, M. (Eds.), 2008. From Control to Design: Parametric/Algorithmic Architecture. Actar, Barcelona, Spain.

Schmidt, B., Fraternali, F., Ortiz, M., 2009. Eigenfracture: an eigendeformation approach to variational fracture. Multiscale Model. Simul. 3, 1237–1266.

Skelton, R.E., 2002. Structural systems: a marriage of structural engineering and system science. J. Struct. Control 9, 113–133.

Skelton, R.E., de Oliveira, M.C., 2010a. Optimal complexity of deployable compressive structures. J. Franklin Inst. 347, 228–256.

Skelton, R.E., de Oliveira, M.C., 2010b. Optimal tensegrity structures in bending: the discrete Michell truss. J. Franklin Inst. 347, 257–283.

Skelton, R.E., de Oliveira, M.C., 2010c. Tensegrity Systems. Springer, New York, NY, USA.

Skelton, R.E., Nagase, K., 2012. Tensile tensegrity structures. Int. J. Space Struct. 27, 131–137.

Sokóf, T., Rozvany, G.I.N., 2012. New analytical benchmarks for topology optimization and their implications. Part I: bi-symmetric trusses with two point loads between supports. Struct. Multidisc Optim. 46, 477–486.

Tilbert, A.G., Pellegrino, S., 2011. Review of form-finding methods for tensegrity structures. Int. J. Space Struct. 18, 209–223.

Yamamoto, M., Gan, B.S., Fujita, K., Kurokawa, J., 2011. A genetic algorithm based form-finding for tensegrity structure. Procedia Eng. 14, 2949–2956.